


**Interaction-induced spatial correlations in a disordered glass**Z. Ovadyahu *Racah Institute of Physics, The Hebrew University, Jerusalem 9190401, Israel*

(Received 22 March 2022; accepted 18 May 2022; published 2 June 2022)

A consequence of the disorder and Coulomb interaction competition is the electron-glass phase observed in several Anderson insulators. The disorder in these systems, typically degenerate semiconductors, is stronger than the interaction, more so the higher is the carrier concentration  $N$  of the system. Here we report on a feature observed in the electron-glass phase of  $\text{In}_x\text{O}$  with the lowest  $N$  yet studied. The feature, resolved as a broad peak in field-effect measurements, has not been recognized in previously studied Anderson insulators. Several empirical facts associated with the phenomenon are consistent with the conjecture that it reflects a correlated charge distribution. In particular, the feature may be turned on and off by gate-voltage maneuvering, suggesting the relevance of charge arrangements. It may also be suppressed by either temperature, non-Ohmic field, or exposure to infrared illumination. After being washed out, the feature reappears when the system is allowed to relax for sufficiently long time. A puzzling aspect that arises is the apparent absence of the phenomenon when the carrier concentration increases above a certain value. This is reminiscent of the glass-transition conundrum, except that the role of temperature in the latter is played by disorder. Analysis of these findings highlights several issues that challenge our understanding of the disorder-interaction interplay in Anderson insulators.

DOI: [10.1103/PhysRevB.105.235101](https://doi.org/10.1103/PhysRevB.105.235101)**I. INTRODUCTION**

The interplay between disorder and Coulomb interactions has been the subject of intense research, mostly devoted to degenerate Fermi systems [1–4]. A common feature observed in disordered-interacting condensed-matter systems is a local depression in their single-particle density of states  $\rho(\varepsilon)$ . This feature, referred to as a zero-bias anomaly (ZBA), is anchored to the chemical potential of the system and appears in both the diffusive [5,6] and insulating regimes [7,8]. A zero-bias anomaly may be observed when inserting a particle into the many-body system faster than the time it takes existing particles to relax to its presence. This may be accomplished in a tunneling or photoemission measurement of disordered metals and doped semiconductors. When the system is quantum coherent, the process is closely related to the Anderson orthogonality catastrophe [9].

An indirect way to monitor  $\rho(\varepsilon)$  becomes possible in systems where the disorder exceeds the critical value for Anderson localization; the competition between disorder and the unscreened Coulomb interaction slows down the medium relaxation which, in turn, makes the system  $\rho(\varepsilon)$  observable in field-effect experiments [10–18]. In this case a ZBA appears as a modulation of the conductance versus gate voltage,  $G(V_g)$  [14]. This feature, called a memory dip (MD), has been observed in several heavily doped semiconductors where the disorder necessary to render them Anderson insulators is large enough to reduce electronic relaxation rates many decades below the transition times associated with their conductivity [19]. Anderson insulators in this group exhibit glassy dynamics and are referred to as electron glasses. These should be distinguished from lightly disordered

systems (sometimes called Coulomb glasses) that do not exhibit MD in field-effect experiments [19]. The relation between the single-particle density of states and the MD has been elucidated in Refs. [12,14,17,18].

Theoretical models that incorporate disorder and interactions are usually concerned with the low-energy part of the single-particle density of states. The energy locations of the states that were expelled from the ZBA region have received less attention. In particular, in the Anderson-localized regime, where  $\rho(\varepsilon)$  has traditionally been derived via a classical Coulomb-gap approach, the missing states are usually depicted as being evenly spread outside the depleted region [20–23]. Given that disorder in Anderson insulators is in general significantly stronger than the Coulomb interaction [24], this picture seems plausible and is consistent with results of tunneling [25,26] and field-effect experiments on strongly disordered systems [27].

Recently, however, a strikingly different behavior was detected in a particular version of amorphous indium-oxide  $\text{In}_x\text{O}$  films, as shown in Fig. 1. The MD exhibited by a specimen of this version reveal a structure that resembles that of a superconductor  $\rho(\varepsilon)$  with its characteristic coherence peaks at the edges of the ZBA. The version of  $\text{In}_x\text{O}$  used in this work is *not* superconducting (at least down to  $\approx 0.28$  K) even when the system is in the diffusive transport regime [28]. Moreover, the indium-rich version of  $\text{In}_x\text{O}$ , which *is* superconducting when its disorder is sufficiently small, does show a memory dip when strongly localized but without these side shoulders [27]. Different versions of  $\text{In}_x\text{O}$  are distinguished by their In/O composition that determines their carrier concentration  $N$  [28]. In terms of microstructure they are quite similar. Electron-diffraction patterns of the superconducting version

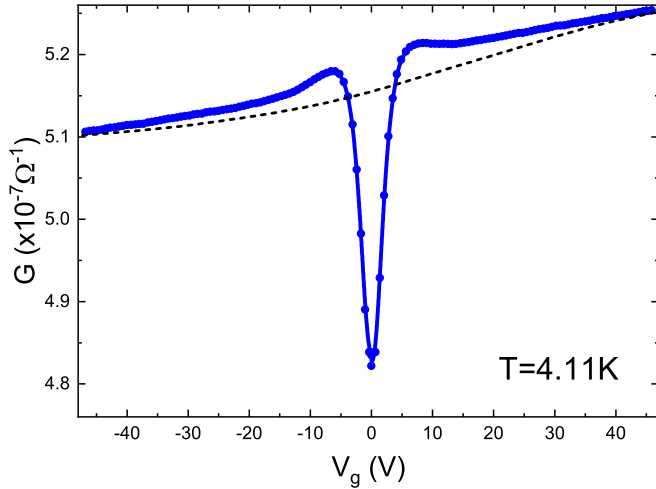


FIG. 1. Conductance  $G$  vs gate voltage  $V_g$  for a 20-nm-thick  $\text{In}_x\text{O}$  film with carrier concentration  $N \approx 10^{19} \text{ cm}^{-3}$ . The sample is separated from a degenerate Si:B gate by  $2\text{-}\mu\text{m}$  layer of  $\text{SiO}_2$ . The figure shows a memory dip centered at  $V_g = 0$ , where the sample was equilibrated for an hour after being cooled from room temperature. The dashed line delineates the energy dependence of  $\partial n/\partial \mu$ , the material thermodynamic density of states.

of the compound and that of the low-carrier-concentration sample used in this study are shown in Fig. 2. A scan of the radial intensity distribution of these patterns shown in Fig. 3 is required to be able to detect any difference between the two versions. Detailed study of the  $\text{In}_x\text{O}$  versions, including x-ray diffraction and interferometry, and Raman spectrometry showed that in terms of structural properties, different versions only differ by small quantitative aspects like the position of the boson peak [29]. However, in terms of disorder perceived by the charge carriers, the difference may be substantial when comparing  $\text{In}_x\text{O}$  with similar resistivities but different carrier concentrations. The system with the lower carrier concentration has a lower disorder (given the same resistivity), and therefore it may also be more homogeneous.

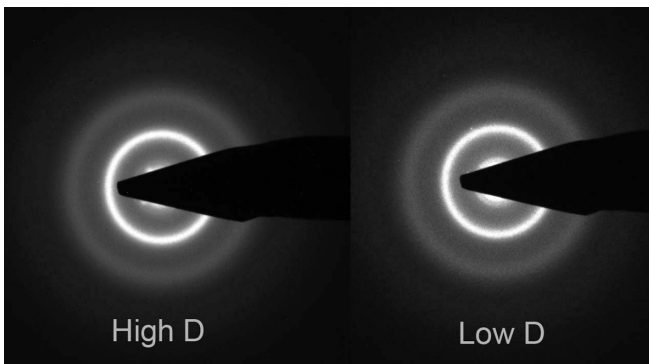


FIG. 2. Electron diffraction patterns of two versions of  $\text{In}_x\text{O}$  films 20 nm thick. The left pattern (marked High D) has carrier concentration  $N \approx 8 \times 10^{20} \text{ cm}^{-3}$  the right pattern (marked Low D) is characteristic of the batch used in the present study with  $N \approx 10^{19} \text{ cm}^{-3}$ .

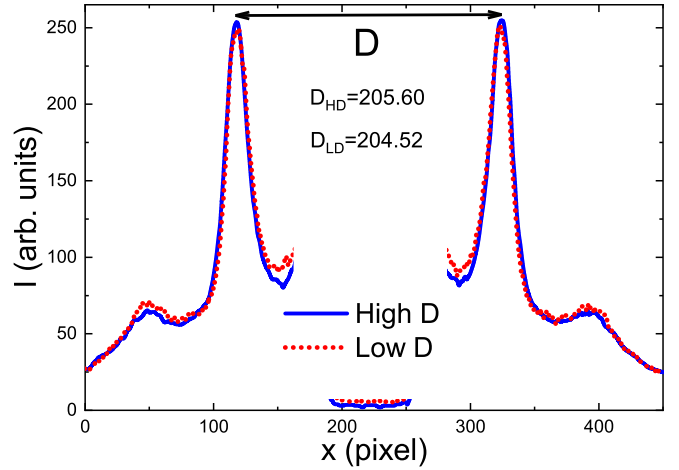


FIG. 3. Intensity profile scan of the two diffraction patterns shown in Fig. 2. The first ring diameters (in units of pixels) are shown for comparison. Note the similarity and the small difference in the nearest-neighbor distance of the two versions.

Theoretically, piling up of states at the edges of the ZBA is consistent with the sum rule for  $\rho(\epsilon)$ . A nonmonotonic  $\rho(\epsilon)$  above the gap was demonstrated in numerical studies of disordered and interacting quantum systems, explicitly in strongly correlated compounds [30–34] and in quantum dots [35]. A “shouldered”  $\rho(\epsilon)$ , quite similar in shape to the MD exhibited in Fig. 1, was obtained in Monte Carlo simulations based on a random-displacement version of the Coulomb glass [36–38]. The shoulders in this scenario were related to a charge-ordering process in the spirit of formation of a “disordered” Wigner crystal or, perhaps more appropriately, a “Wigner glass” [39–42]. The visibility of shoulders in [36] is exponentially reduced with the disorder strength  $W$ . Consequently, this feature has been resolved in the simulations only for  $W$  much smaller than the Coulomb interaction amplitude  $E_C$  [38,43]. By contrast, the ratio  $W/E_C$  in Anderson insulators with Gaussian disorder is typically larger than unity [24]. In the sample shown in Fig. 1, for example, this ratio is estimated to be  $\approx 6$ , which, according to numerical simulations [36,38], seems unfavorable for a charge-ordering mechanism to be effective. To account for a “shouldered MD” (SMD), it may perhaps be necessary to take additional factors into account than included in the considerations used for the classical Coulomb glass.

We present in this work extensive data pertaining to this phenomenon and offer a heuristic interpretation for the main effects that characterize it. Some puzzling issues that need further experimental and theoretical elucidation are pointed out.

## II. EXPERIMENTAL

### A. Sample preparation

The samples used in this study were amorphous indium-oxide ( $\text{In}_x\text{O}$ ) films made by e-gun evaporation of 99.999% pure  $\text{In}_2\text{O}_{3-x}$  onto room-temperature Si wafers in a partial pressure of  $1.3 \times 10^{-4}$  mbar of  $\text{O}_2$  and a rate of  $0.3 \pm 0.1 \text{ \AA/s}$ . Under these conditions the carrier concentration  $N$  of the

samples, measured by the Hall effect at room temperature, was  $N \approx (1 \pm 0.1) \times 10^{19} \text{ cm}^{-3}$ . Using a free-electron formula, this carrier concentration is associated with  $\partial n / \partial \mu \approx 10^{32} \text{ erg}^{-1} \text{ cm}^{-3}$ . The Si wafers (boron doped with bulk resistivity  $\rho \leq 2 \times 10^{-3} \Omega \text{ cm}$ ) were employed as the gate electrode in the field-effect experiments. A thermally grown  $\text{SiO}_2$  layer,  $2 \mu\text{m}$  thick, served as the spacer between the sample and the conducting Si:B substrate. The screening length of the material  $\lambda \approx (\pi e^2 \partial n / \partial \mu)^{-1/2}$  is  $\approx 2 \text{ nm}$ , and therefore the voltage that actually affects the sample is  $\approx 10^{-3}$  of  $V_g$ , the voltage applied between the sample and the gate. At room temperature the sheet resistance of the samples used here ranged between 22.5 and 25 k $\Omega$ .

The film thickness was measured *in situ* by a quartz crystal monitor calibrated against x-ray reflectometry. Sample geometry was defined by the use of a stainless-steel mask during deposition into rectangular strips  $0.9 \pm 0.1 \text{ mm}$  long and  $1 \pm 0.1 \text{ mm}$  wide. Four different batches were made in this study, and here we report detailed results of three different samples from one of these batches with a thickness of  $20 \pm 5 \text{ nm}$ . The dimensionless parameter  $k_F \ell$  for these samples is 0.27–0.29, just on the insulating side of the critical value for this material ( $0.31 \pm 0.1$  [28]).

### B. Measurement techniques

Conductivity of the samples was measured using a two-terminal ac technique employing a 1211 ITHACO current preamplifier and a PAR 124A lock-in amplifier using frequencies of 64–71 Hz depending on the RC of the sample-gate structure.  $R$  is the source-drain resistance and  $C$  is the capacitance between the sample and the gate.  $C$  in our samples was typically  $\cong 10^{-10} \text{ F}$ , and  $R$  for the samples studied in this work ranging between 1.5 and 2.5 M $\Omega$  at 4.11 K. Except when otherwise noted, the ac voltage bias in conductivity measurements was small enough to ensure near-Ohmic conditions. Except where otherwise noted, measurements were performed with the samples immersed in liquid helium at  $T \approx 4.11 \text{ K}$  held by a 100-L storage dewar. This allowed up to 2 months measurements on a given sample while keeping it cold and in the dark. These conditions are essential for measurements where extended times of relaxation processes are required at a constant temperature. Fuller details of the field-effect measurement setup, sample configuration, and characterization are described in [29]. An up-to-date list of the studied Anderson insulators that exhibit a memory dip along with a description of their systematic dependence on the carrier concentration of the material are given in [19].

## III. RESULTS AND DISCUSSION

### A. The basic facts associated with the SMD

The SMD state is sensitive to the conditions under which it is measured in the field-effect experiment. In particular, sweeping  $V_g$  over a range  $|\Delta V_g|$  that exceeds the typical width  $\Gamma_S$  of the shoulder results in a shoulderless MD when a  $V_g$  sweep is taken again along the original interval and polarity. The protocol used throughout this work to achieve this state (labeled as “reference”) involves sweeping  $V_g$  from 0 to +70 V and back to 0 V, and then the sample is relaxed at this

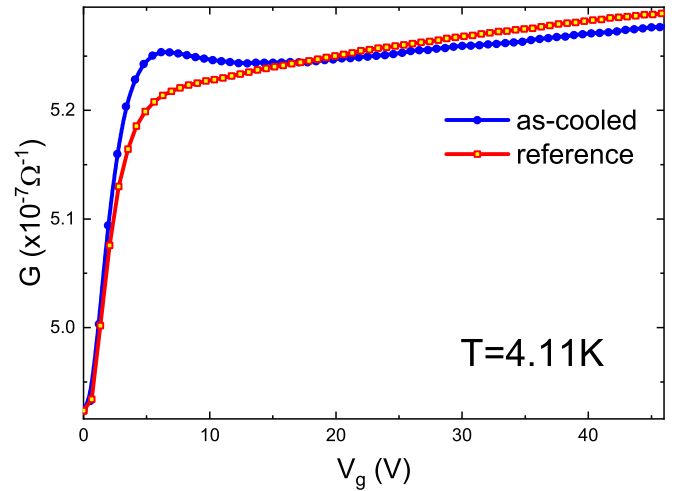


FIG. 4. Field-effect scans comparing the reference, shoulderless state (see text) with the  $G(V_g)$  of the sample 20 min after being quench-cooled from room temperature to the bath temperature. The two plots were taken with the same scan rate  $\partial V_g / \partial t$  of 1.2 V/s.

position for 20 min allowing the ZBA to reform before taking the next  $G(V_g)$  scan. An example is illustrated in Fig. 4.

However, this shoulderless  $G(V_g)$  turns out to be metastable; the SMD state of the sample reappears if one lets the sample equilibrate under the initial  $V_g$  for long enough time before taking a new sweep. The recovery of the SMD is illustrated in Figs. 5 and 6 for the right-hand and left-hand side  $G(V_g)$  scans, respectively. These time-dependent data imply that the SMD state has a lower energy than the reference state.

The dynamics associated with the SMD “rejuvenation” process described by the data in Figs. 5 and 6 differs from that exhibited by that of the electron-glass relaxation process

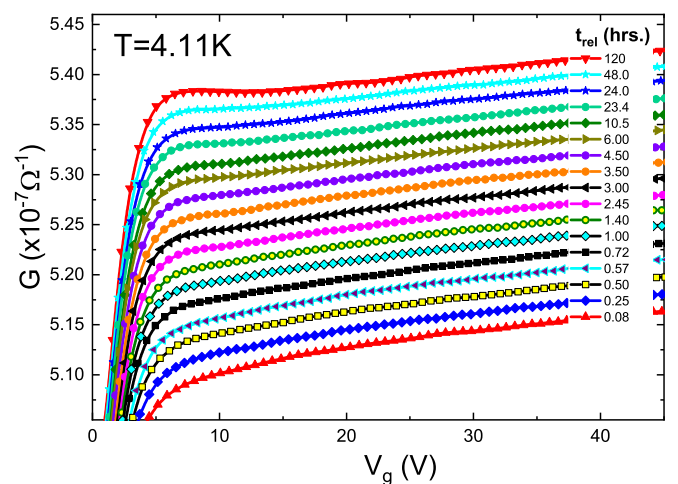


FIG. 5. The recovery of the SMD state with relaxation time  $t_{\text{rel}}$  starting from a “reference” state at  $t = 0.08 \text{ h}$ . Data are shown here for the right-hand side of the field effect. Before taking each plot, a new reference state was prepared by sweeping the gate voltage to +70 V and back to 0 V. The plots are displaced along the ordinate for clarity, and each was taken with the same sweep rate of  $dV_g / dt = 1.2 \text{ V/s}$ .

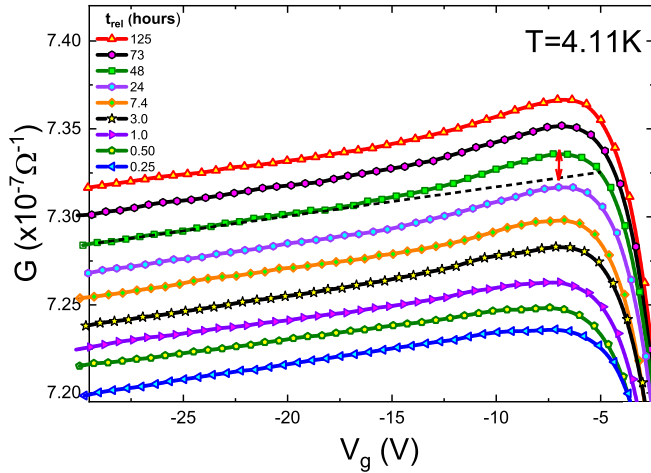


FIG. 6. The recovery of the SMD state as function of the relaxation time  $t_{\text{rel}}$  starting from a reference state at  $t = 0.25$  hours. Data are shown for the left-hand side of the field effect. Before taking each plot, a new reference state was prepared by sweeping the gate voltage to  $+70$  V and back to  $0$  V. The plots are displaced along the ordinate for clarity. All plots were taken with the same sweep rate of  $dV_g/dt = 1.2$  V/s. The dashed line and the red arrow delineate the way we define the magnitude of the shoulder at a given  $t_{\text{rel}}$  (see text and Fig. 7).

monitored through the conductance  $G(t)$  which, characteristically, is logarithmic [27]. The two types of relaxations are compared in Fig. 7 for one of the samples.

Note first that the SMD evolution persists and is followed for two more decades in time than the conductance relaxation. The main part of the change in  $G(t)$  is over while that of  $\Delta G$  is still building up. Secondly, although the two processes are probably related (and begin and end essentially at the same times), the functional time dependence of  $\Delta G(t)$  being stretched exponential with exponent  $\beta = 0.78$  suggests a process dominated by a relatively narrow rate distribution [44]. This point will be clarified below.

The disparity in the dynamics of the two types of slow relaxations is also manifested in the dependence of the SMD magnitude on the sweep rate. This is shown in Fig. 8 for another sample in the batch studied. Note that  $\Delta G$ , the depth of the ZBA in these plots is changing substantially with the sweep rate [Fig. 8(a)] owing to the relative fast relaxation dynamics of these samples. The logarithmic dependence of  $\Delta G$  on the sweep rate is a common feature in electron glasses [45]. This dependence carries over to the ratio  $\delta G/\Delta G$  [where  $\delta G$  is the shoulder height, see Fig. 8(b)] because of the much weaker change of  $\delta G$  with the sweep rate.

### B. The shoulder origin—A heuristic interpretation

Based on the data presented above, it is conjectured that the shoulders reflect an increase in the density of states at the edges of the MD in the same vein that the depression of  $G(V_g)$  signifies a depletion of charge at the chemical potential set by  $v_g^{\text{eq}}$ , the equilibrium gate voltage. The MD has been related to the soft gap at  $\rho(\epsilon)$  resulting from the long-range Coulomb interaction [12–14,17–19,45].

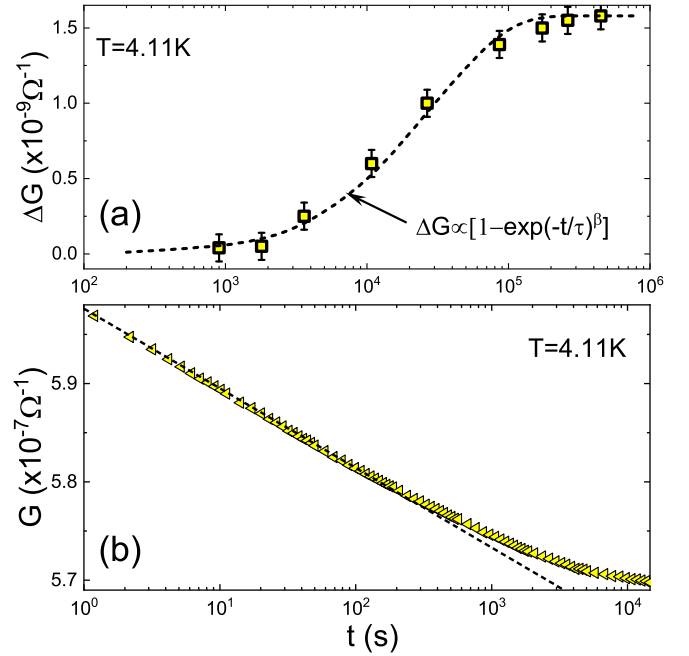


FIG. 7. (a) The recovery of the shoulder with time characterized by  $\Delta G$  defined by the construction shown in Fig. 6 as a red arrow. The dashed line in the figure is a fit to the stretched-exponential function with  $\beta = 0.78$  and  $\tau = 23\,400$  s. (b) The relaxation of this sample conductance monitored by recording  $G(t)$  at  $V_g = 45$  V after changing the gate voltage from the equilibrium state at  $0$  V to  $45$  V. The dashed line delineates the logarithmic relaxation law. Note the two-decades difference in timescales between the two plots.

On its own, the interaction favors a correlated spatial distribution of the states expelled from the low energy of  $\rho(\epsilon)$ . Therefore a lower energy configuration should be attained when the distribution of the nearest-neighbor distances is peaked at a value of the order  $N^{-1/3}$ , where  $N$  is the system carrier concentration. This in turn would show up as a peak in  $G(V_g)$  at  $E_C \approx e^2 N^{1/3}/\kappa$ , where  $\kappa$  is the effective dielectric constant of the medium. The shoulder in our samples is peaked at  $E_C \approx 7$  meV, and it tapers off towards  $\approx 40$ – $50$  meV (Fig. 1). For the batch used here,  $N \approx 10^{19}$  cm $^{-3}$ , the observed peak of the shoulder is consistent with  $E_C \approx e^2 N^{1/3}/\kappa$  if  $\kappa \approx 45$ . The bare dielectric constant of the material is  $\kappa \approx 10$ , but the polarization of localized states may enhance it to be consistent with this scenario.

To further assess the plausibility of this picture, we need to consider the role of disorder. The precondition for the MD to be observable in the field-effect experiment is a strong enough disorder [19]. Explicitly, the disorder has to be strong enough to Anderson-localize the system *and* to render its relaxation slower [19] than the sweep rate of  $V_g$ . On the other hand, too strong a disorder would defeat the electron-electron tendency to form an ordered structure and randomize the states spatial distribution, thus suppressing the shoulder. Intuitively, out of the systems that exhibit MD, the best candidate to show shoulders is where the disorder to interaction ratio is small. This favors systems with low carrier concentration  $N$ , because the disorder necessary to Anderson localize a system increases with its Fermi energy  $E_F \propto N^{2/3}$ , while the interaction scales

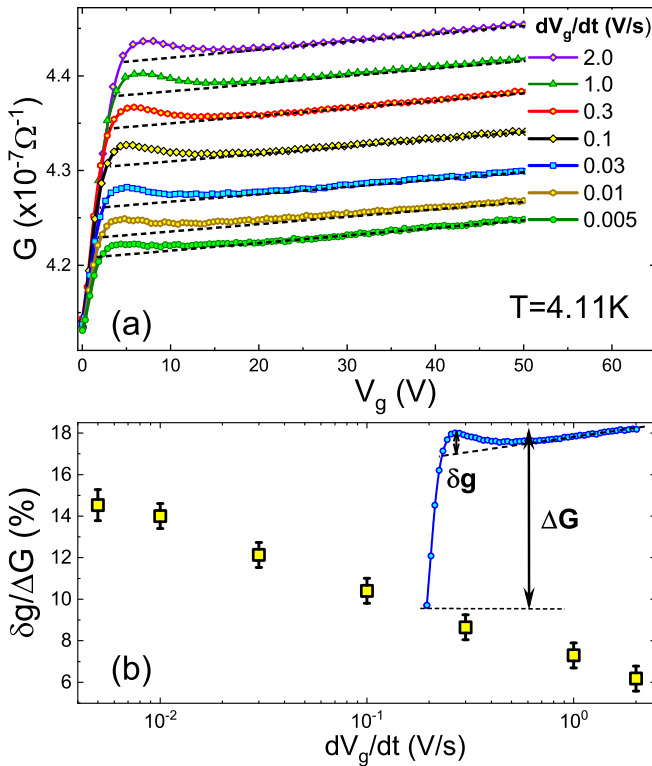


FIG. 8. (a) Dependence of the SMD plots on the gate-voltage sweep rate  $dV_g/dt$ . (b) The magnitude of the shoulder relative to that of the MD, defined as shown in the inset, as a function of the sweep rate  $dV_g/dt$ .

with  $N^{1/3}$ . Note that the SMD discussed here has the lowest  $N$  among all the electron-glass systems yet reported [19,46]. This may be in line with our charge-ordering scenario in the sense that the present system has more favorable parameters than previously studied electron glasses to show shoulders in field-effect measurements.

But how favorable are the actual system parameters? The magnitude of the interaction identified above with the position of the shoulder was  $E_C \approx 7$  meV. The relevant [47] disorder  $W$  may be estimated from the width of the shoulder (Fig. 1), yielding  $W/E_C \approx 6$ . The disorder-to-interaction ratio typical for a degenerate semiconductor ranges between  $\approx 3$  and 100 [24]. As anticipated, the current system is at the “favorable” limit in terms of parameters. Yet this ratio is far from the  $W/E_C \ll 1$  limit, where shoulders are observed in classical simulations [36–38]. Hopefully the results reported here may assist in identifying the missing ingredients from these simulations.

The presence of disorder is also essential for understanding the time-dependent processes depicted in Figs. 5 and 6; sweeping the gate voltage by a  $|\Delta V_g| > \Gamma_S$  (where  $\Gamma_S$  is the shoulder width) results in a shoulderless state (Fig. 4). However, given time, the shoulder is sluggishly recovered and  $G(V_g)$  eventually exhibits the SMD behavior. Presumably, the metastable MD state is made up of charges trapped by disorder over the voltage range swept by the gate. Some of the charges that were driven by the gate to occupy higher-energy states are trapped by deep wells of the potential while the gate travels

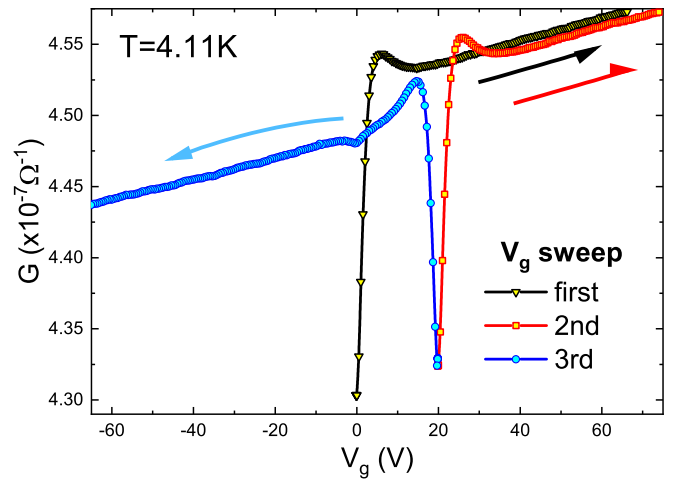


FIG. 9.  $G(V_g)$  plots taken consecutively. First,  $V_g$  was swept from the original equilibrium  $v_g^{\text{eq}} = 0$  V to +65 V (triangles). This is followed by sweeping  $V_g$  to +20 V and parking there for 20 min. Next,  $V_g$  was swept to +80 V (squares).  $V_g$  was then moved to +20 V and parked there for 20 minutes to relax. Finally,  $V_g$  was swept to -65 V (circles). Note that the latter  $G(V_g)$  plot was taken less than an hour after the first sweep, and the magnitude of the MD at  $V_g = 0$  V has shrank by a factor of  $\approx 60$  relative to the original value. All plots were taken with the same  $dV_g/dt = 0.5$  V/s.

back to  $v_g^{\text{eq}}$ . Charges occupying states with shallow wells of the potential will escape these states during the time the gate is set back in  $v_g^{\text{eq}}$  to rebuild the MD for the next  $G(V_g)$  run. This explains both the shifting of charge away from the shoulder towards higher energies and the relative absence of the fast relaxation rates in the relaxation associated with the shoulder recovery.

The proposed picture for creating the shoulderless state is analogous to the process by which debris is washed ashore by sea waves and is held on the beach slope by friction when the wave pulls back seaward.

Despite the apparent difference in their dynamics, it is clear that the shoulder and the memory dip are two parts of the same phenomenon; when the equilibrium voltage is moved, so is the position of the shoulder. An example illustrating the “two-dip experiment” [46] for the current batch of  $\text{In}_x\text{O}$  is shown in Fig. 9.

The feature that strikes the eye in Fig. 9 is the barely discernible MD produced in the third sweep at the original  $v_g^{\text{eq}} = 0$  V. The magnitude of this MD is smaller by almost two orders of magnitude relative to either of the two “fresh” MDs. This is due to the relatively fast dynamics of this weak-disorder batch [19,46,48]. A closer look at the figure reveals a new aspect of the phenomenon; establishing a new  $v_g^{\text{eq}}$  (at +20 V) yields at the edge of the MD a prominent shoulder despite being in the voltage range covered by  $V_g$  in a previous sweep. In a way, this is similar to the shoulders appearing along with the MD upon the first cooldown from room temperature. Both the MD and the shoulder appear in this case after a brief relaxation period (typically 20 min); no days-long waiting time is required. In fact, as will be shown next, once new equilibrium conditions are set, the full SMD appears in the  $G(V_g)$  plot.

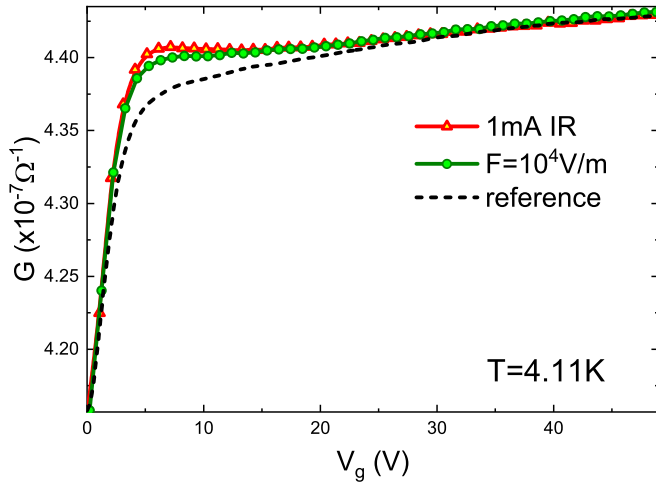


FIG. 10. Field-effect plots illustrating two examples of the shoulder reappearance following a quench from a nonequilibrium, higher-energy state. Stressing the sample with a non-Ohmic field  $F = 10^4$  V/m held on for 20 min (circles), and exposing the sample to 1 mA of the IR source for 3 s (triangles). In both cases the shown  $G(V_g)$  plots are taken after letting the sample relax for 20 min since the respective quench. These are contrasted with the reference plot produced after a scan to +70 V. All three plots were measured in the linear response and with the same  $dV_g/dt = 1$  V/s.

### C. Shoulder destruction and rejuvenation

As shown above, taking a  $G(V_g)$  measurement over a  $V_g$  range larger than  $\Gamma_S$  eliminates the shoulder from showing up in the next scan. A prolonged relaxation of the sample is required for its recovery. However, there are several ways to restore the SMD without a long time delay. Two of these were mentioned in the paragraph above. Three other schemes effective in rejuvenating the shoulder are described next.

The SMDs resulting from applying the first two are illustrated in Fig. 10. Both schemes produce shoulders that exhibit higher visibility than would be expected by allowing the system to relax at  $v_g^{\text{eq}}$  for the time required for completing the scheme (compare with Fig. 5).

The third scheme is the easiest to implement, and it turns out to be the most effective in pulling back the shoulder from the reference state. In this case,  $V_g$  is first swept to  $V_g = -|v_g^{\text{bias}}|_1$ , staying there for  $\approx 2$  s, and then set back at  $V_g = 0$  V for 20 min relaxation before recording a  $G(V_g)$  plot from 0 to +60 V. As noted before, this trip erases the shoulder. This “ $v_g^{\text{bias}}$ ” protocol is repeated for different (negative) bias values, thus generating plots as a function of  $-|v_g^{\text{bias}}|$ . In each such plot the shoulder is “rejuvenated” by prebiasing the sample with a finite  $-|v_g^{\text{bias}}|$ . These bias values were taken at random order to verify that “history” does not play a role. A series of such plots with  $|v_g^{\text{bias}}|$  values ranging from 5 to 80 V is shown in Fig. 11(a).

Note in Fig. 11(b) that the relative magnitude of the shoulder  $\delta G$  increases with  $|v_g^{\text{bias}}|$  and tends to saturate for  $v_g^{\text{bias}} \approx -50$  V. The range over which the gate-voltage bias affects  $\delta G$  is similar to the typical width of the shoulder  $\Gamma_S$ , which in turn is related to the disorder associated with the phenomenon  $W$ . It is emphasized that these data are generated using random

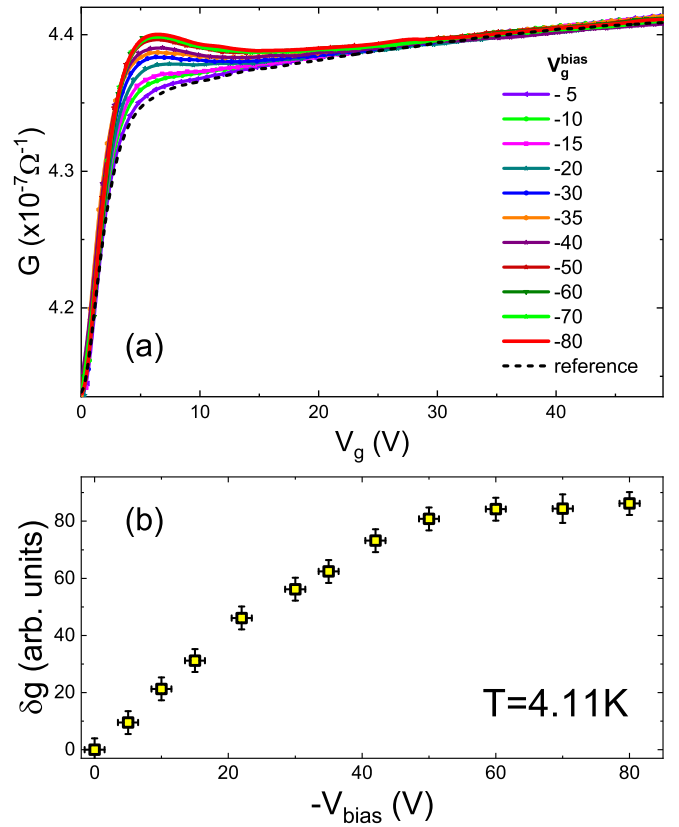


FIG. 11. The reappearance of the shoulder in the  $G(V_g)$  plots recorded by the “ $v_g^{\text{bias}}$ ” protocol described in the text. These are labeled by their prescan (negative) bias (a). The plots were taken consecutively using the same sweep rate  $dV_g/dt = 1$  V/s. (b) The magnitude of the shoulder vs the prebias voltage. This magnitude is taken as the distance from the peak of the shoulder at 6.8 V to the value of the reference curve at this voltage.

values for  $|v_g^{\text{bias}}|$  in the consecutive measurements. Therefore the correlation between  $|v_g^{\text{bias}}|$  and  $\delta G$  is meaningful and suggestive. Actually, these results lead us to recognize the common element in the four different schemes that produces a SMD from a “reference” state: *They all involve a quench from a state where the charge carriers are endowed with excess energy  $E_{\text{excess}}$  relative to the equilibrium state.* These schemes differ by how  $E_{\text{excess}}$  is structured (distributed in energy) relative to  $W$ , which presumably determines its efficiency in pulling up the shoulder. When the excess energy of charge carriers exceeds  $W$ , they are no longer trapped by potential wells of the disorder. Rather, their spatial distribution is controlled by the Coulomb repulsion forcing them apart. In this stage the system is in a fluid, spatially correlated state that, following a quench and brief relaxation, is well primed to form SMD.

The efficiency of a scheme to produce SMD is not necessarily reflected in the conductance enhancement accompanying the process. For example, stressing the sample with a large longitudinal field enhances the sample conductance by a factor of  $\approx 2$ , while the shoulder that results from this scheme is visibly weaker (Fig. 10) than that obtained by the brief IR illumination that had a much smaller impact on the conductance [see Figs. 12(a) and 12(b)].

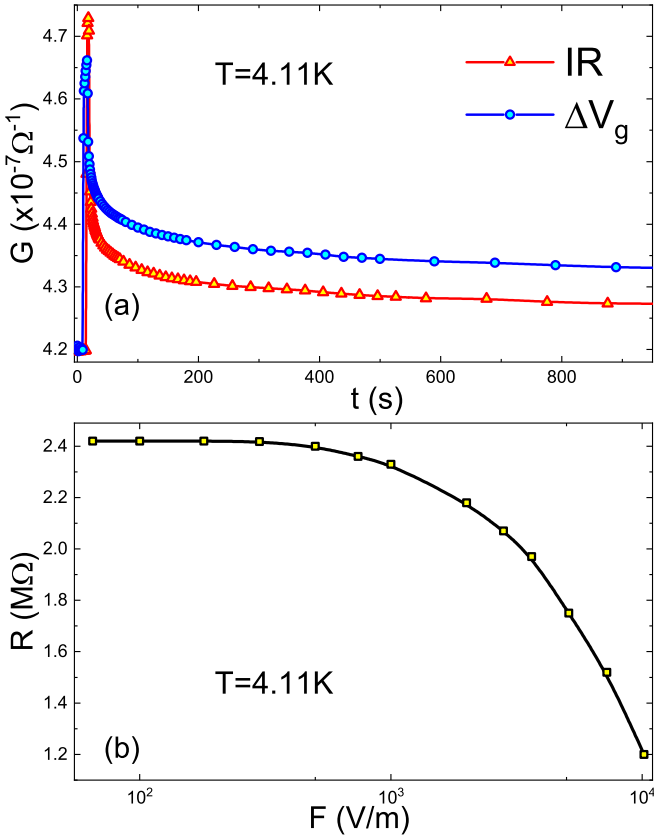


FIG. 12. The effects produced on the sample by a brief IR illumination and a large applied electric-field. (a) The conductance increase and subsequent relaxation in response to a 3-s exposure to the 1-mA IR source. This is compared to the similar effect produced by a sudden change of the gate voltage from 0 to 45 V (a 5-s trip time). (b) The sample resistance as a function of the applied electric field.

### 1. Temperature dependence

Temperature has a marked effect on the electron-glass features. Both the width of the memory dip and its relative magnitude are systematically affected by raising the temperature [49]. Here it is shown that the shoulder follows the same trend; its peak is slightly shifted towards a higher  $V_g$  upon increasing the bath temperature, and its magnitude is exponentially suppressed [Fig. 13(b)]. This temperature dependence was obtained before in the electron-glass phase of  $\text{In}_2\text{O}_{3-x}$  films [49]. Apart from reaffirming that the shoulder is an integral part of the memory dip, it illustrates how sensitive the visibility is to the addition of high-energy components.

### 2. Nonequilibrium steady state under IR illumination

Even more striking is the effect of a continuous IR illumination, which suppresses the shoulder despite the extremely weak power load on the sample (Fig. 14). Under a continuous IR illumination the sample SMD magnitude was reduced to half its dark value while the conductance increased by only  $\simeq 2.8\%$  [see Fig. 14(a)]. Based on the conductance versus temperature of this sample shown in Fig. 15, this is the equivalent of raising the temperature by  $\approx 20$  mK. To achieve a similar reduction of the SMD magnitude of the same sample, the bath

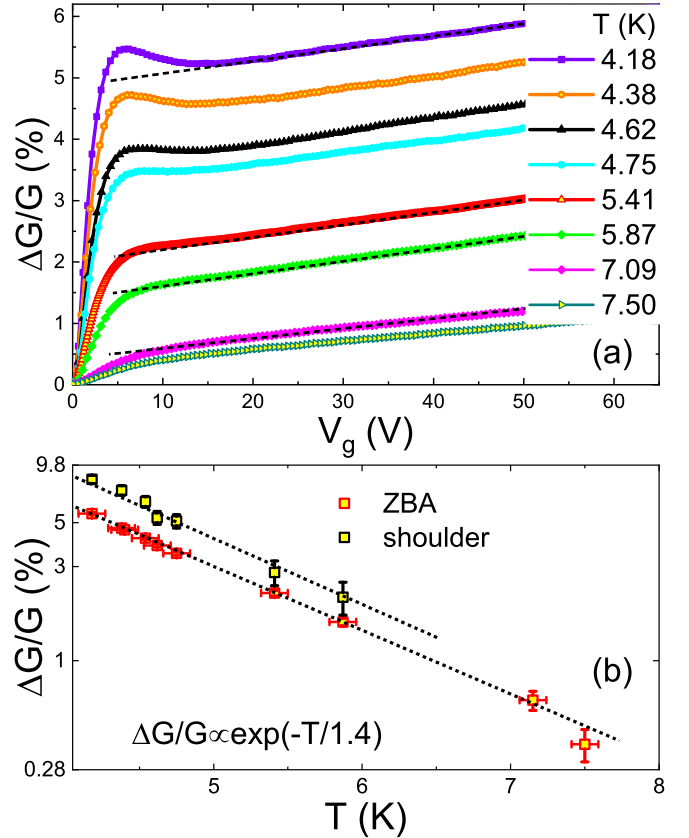


FIG. 13. (a) The dependence of the  $G(V_g)$  plot on temperature for a typical SMD sample. Each plot was taken after first sweeping the gate to  $-70$  V and back to 0 V to allow shoulder rejuvenation (see text) and relaxation. Then the bath temperature was changed and the same protocol repeated with  $V_g/dt = 0.5$  V/s. (b) The relative magnitude of the ZBA and the shoulder extracted from the data in (a).  $\Delta G/G$  for the ZBA is the value of  $G(V_g)$  at  $V_g = 7$  V.  $\Delta G/G$  values for the shoulder are taken as in Fig. 6 relative to the dashed lines in (a). Dotted lines fit  $\exp[-T/1.4]$  (see text). Note that both axes in plot (b) use a logarithmic scale.

temperature must be raised to  $T \simeq 5.5$  K (see Fig. 13), which increases the conductance by  $\simeq 300\%$ .

The difference between these two protocols is in how the energy added to the system is distributed among the available degrees of freedom. Under the IR illumination, the system is populated with an excess of high-energy phonons. These are generated by a cascade process: Electrons are excited to high energy, then relax by optical phonon emission [50]. This nonequilibrium steady state has much fewer low-energy phonons than when the sample is heated up to  $\approx 5.5$  K. The density of high-energy phonons is also increased by raising the bath temperature, but most of the absorbed energy is spent on enhancing the conductance. The indication is that the SMD state is sensitive to the presence of high-energy phonons. This may hint on an underlying mechanism that counteracts the disorder in the competition with interactions. High-energy phonons is a potent source of dephasing, which raises the possibility that quantum effects play a role. Effects that hinge on quantum coherence and may be relevant to the problem at hand are those that promote spatially extended

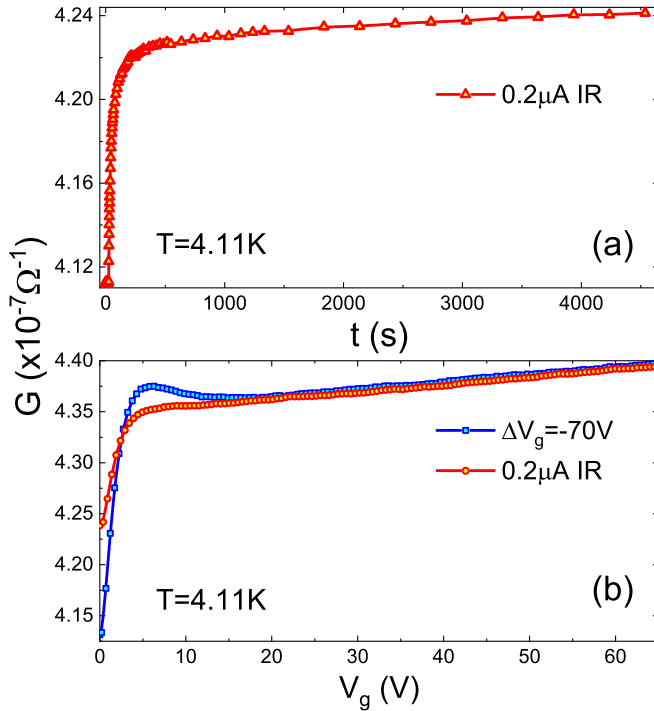


FIG. 14. (a) Sample conductance vs time while being exposed to IR radiation with a constant power of  $2 \times 10^{-7}$  W. Note that  $G(t)$  tends to reach a saturated value for  $t \gtrsim 1$  h. (b) The sample  $G(V_g)$  plot in the dark (squares) compared with the  $G(V_g)$  plot taken under the constant IR illumination after the conductance reached “saturated” conditions (explicitly, the change with time for the duration of the  $G(V_g)$  plot is negligible). Both curves were taken after first sweeping  $V_g$  to  $-70$  V, then relaxing the sample for 20 min, and  $dV_g/dt = 0.5$  V/s.

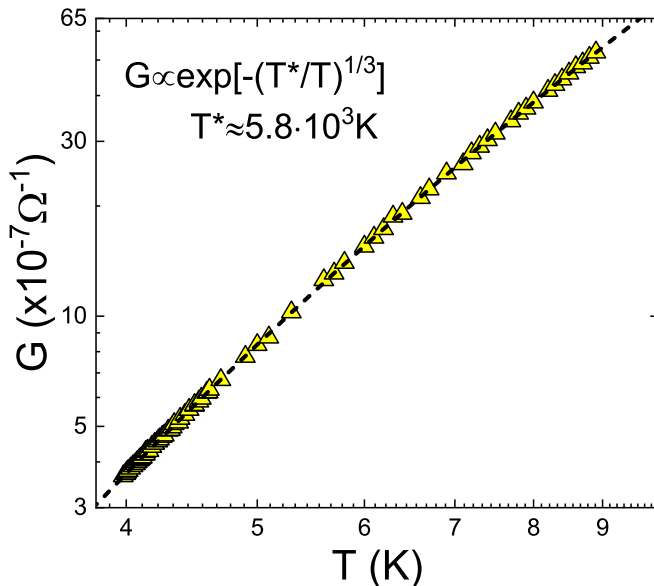


FIG. 15. The temperature dependence (on a double-log scale) of the conductance for the sample used in Figs. 8–14 inclusive.

wave-function-like resonances [51–53] and other wave-function forms resulting from hybridization. The existence of extended wave functions naturally mimics a weaker disorder. There is already evidence for quantum coherence in this system [50,55], so there is reason to further explore this direction.

#### D. Discussion

There are several issues related to the appearance of the shoulders that need to be further clarified. First is the absence of this feature in other versions of  $\text{In}_x\text{O}$ . In contrast with the samples reported here, all studied Anderson-insulating  $\text{In}_x\text{O}$  samples with  $N$  ranging from  $\approx 4 \times 10^{19} \text{ cm}^{-3}$  to  $\approx 8 \times 10^{21} \text{ cm}^{-3}$  exhibit electron-glass characteristics with MD magnitude and width varying systematically with  $N$  but without shoulders [19,27,48]. It seems, therefore, that for  $\text{In}_x\text{O}$ , as  $N$  increases from  $\approx 1 \times 10^{19} \text{ cm}^{-3}$  to  $\approx 4 \times 10^{19} \text{ cm}^{-3}$ , the structure manifested by the shoulders melts away. In terms of In/O ratio, which is the way  $N$  is determined in the compound, this range is merely  $\approx 2\%$  wide [28]. It would be interesting to fine-tune the system  $N$  and track the evolution of the phenomenon across this region. This is a much harder undertaking than it may seem and will require establishing a new level of material deposition and post-treatment control. Nonetheless, on the basis of what is already established, this SMD  $\rightarrow$  MD transition is surprisingly sharp.

It appears that one has to decide between two possibilities: Either the transition is a real phase change, or it is a crossover to a regime with ultraslow dynamics. Explicitly, as  $N$  increases, the shoulders dynamics becomes too slow to be resolved on a realistic timescale. This dilemma is similar to the quandary that has haunted the glass community [54], and perhaps it may take as long to reach a conclusion. In the present case the possibility of a diverging relaxation time has empirical support. The relaxation time of  $\text{In}_x\text{O}$  electron glasses with  $N \approx 4 \times 10^{19} \text{ cm}^{-3}$  to  $N \approx 10^{20} \text{ cm}^{-3}$  was shown to increase dramatically with  $N$  [45,46], and as seen here, the dynamics associated with the shoulders may actually be slower.

Yet, the possibility that the SMD-to-MD changeover is a true phase transition cannot be ruled out either. If the MD  $\rightarrow$  SMD transition is indeed a change between two distinct phases, what are their natures? The SMD state, characterized by a shoulder in the  $G(V_g)$  plot, has been interpreted here as a preponderance of charge at energy of the order  $E_C$  relative to the chemical potential. It is illuminating to contrast this picture with the spatial order of the amorphous structure manifested in the electron-diffraction patterns (Figs. 2 and 3 above). The shoulders and the diffraction pattern represent two amorphous structures—one composed of ions and the other of electronic charges. The first ring in the former is related to the nearest-neighbor distance between ions, which is the analog of the shoulder position in energy. Both the diffraction ring and the shoulder have a width that is a measure of the disorder associated with the respective phenomenon. The diffraction ring is relatively much sharper than the shoulder width. This is due to the difference in the two-particle potential that constrains the spatial freedom of the constituents: Lennard-Jones versus Coulomb interaction for the ions and charge carriers, respectively. For energies outside



the Coulomb gap, this description depicts the SMD state as a “frozen liquid,” while the MD state, lacking “medium-range order,” is a “frozen gas.” The experiments that were performed up to and including this work indicate that there is a transition between these states controlled by the carrier concentration  $N$ . This was ascribed to the competition between disorder and interaction that is tilted in favor of the former when  $N$  increases. To further test this picture, one needs to change disorder, or the interaction, independently, which is a challenging task.

A related issue is the use of lower carrier concentrations than  $N \approx 10^{19} \text{ cm}^{-3}$ . As mentioned above, in the Anderson-localized regime (a precondition to show electron-glass features [19]), both disorder  $W$  and the Coulomb interaction  $E_C$  increase with  $N$ , but  $W \propto N^{2/3}$  while  $E_C \propto N^{1/3}$ , and therefore a lower disorder-interaction ratio is achievable by reducing  $N$ . This, however, has a limited scope; the ratio is a weak function of  $N$  while the dynamics, mainly controlled by  $W$  [19,46], depends on it exponentially. When  $W$  decreases, the relaxation will quickly become too fast for the experimental  $\partial V_g / \partial t$  to expose a memory dip in the field-effect experiments. To our knowledge, there is no Anderson insulator with  $N \lesssim 10^{18} \text{ cm}^{-3}$  that exhibits either MD or SMD.

There are other factors that may be detrimental for charge ordering besides too strong disorder. Obviously, sample inhomogeneity beyond that inherent in the sample disorder (estimated “globally,” usually on the basis of measuring the resistance) will smear out the shoulders even when all other conditions are favorable. In particular, an excess of randomly distributed deep potential wells should be avoided. Generally,

the detailed structure of the background potential, not just its average amplitude, is relevant for the charge-ordering scenario.

A subtle question that is yet to be answered is the effect of a superimposed periodic potential. The effect of underlying crystallinity on the disorder-interaction balance is a pertinent question that may be tested by numerical simulations. However, numerical studies usually use a lattice-model with half-filling, which probably introduces a spatial constraint that likely is incommensurate with the optimal charge arrangement. It is not clear that it may suffice to employ just a very small filling factor in the simulation to capture the physics of charge ordering.

Attempts to answer some of these questions may benefit from further experimental work. Systems that exhibit electron-glass features, such as GeTe,  $\text{Ti}_x\text{O}$ ,  $\text{In}_2\text{O}_{3-x}$ ,  $\text{GeSb}_2\text{Te}_5$ , and Be [19], do not show shoulders in their  $G(V_g)$  plots. It would be useful to know whether this is due to unfavorable  $W/E_C$  or because of their crystallinity. The filling factor in these compounds is naturally small, but their relatively high carrier concentration may be unfavorable. It is worth trying to tweak this by varying their composition. These systems should also be tested for quantum coherence, as this may play a role as alluded to above. A methodical study of these aspects may establish a new platform for the interplay between disorder and interaction in Anderson insulators.

#### ACKNOWLEDGMENTS

Discussions with Oded Agam and Ady Vakin are gratefully acknowledged.

- 
- [1] L. Fleishman and P. W. Anderson, Interactions and the Anderson transition, *Phys. Rev. B* **21**, 2366 (1980); B. L. Altshuler, Y. Gefen, A. Kamenev and L. S. Levitov, Quasiparticle Lifetime in a Finite System: A Nonperturbative Approach, *Phys. Rev. Lett.* **78**, 2803 (1997); D. M. Basko, I. L. Aleiner, and B. L. Altshuler, Metal insulator transition in a weakly interacting many-electron system with localized single-particle states, *Ann. Phys.* **321**, 1126 (2006); I. V. Gornyi, A. D. Mirlin, and D. G. Polyakov, Interacting Electrons in Disordered Wires: Anderson Localization and Low-T Transport, *Phys. Rev. Lett.* **95**, 206603 (2005).
- [2] P. A. Lee and T. V. Ramakrishnan, Disordered electronic systems, *Rev. Mod. Phys.* **57**, 287 (1985), and references therein.
- [3] Daniel C. Tsui, Nobel lecture: Interplay of disorder and interaction in two-dimensional electron gas in intense magnetic fields, *Rev. Mod. Phys.* **71**, 891 (1999).
- [4] I. Mandal and R. M. Nandkishore, Interplay of Coulomb interactions and disorder in three-dimensional quadratic band crossings without time-reversal symmetry and with unequal masses for conduction and valence bands, *Phys. Rev. B* **97**, 125121 (2018).
- [5] A. L. Altshuler and A. G. Aronov, Contribution to the theory of disordered metals in strongly doped semiconductors, *Zh. Eksp. Teor. Fiz.* **77**, 2028 (1979) [*Sov. Phys. JETP* **50**, 968 (1979)]; B. L. Altshuler, A. G. Aronov, and P. A. Lee, Interaction Effects in Disordered Fermi Systems in Two Dimensions, *Phys. Rev. Lett.* **44**, 1288 (1980).
- [6] Y. Imry and Z. Ovadyahu, Density-of-States Anomalies in a Disordered Conductor: A Tunneling Study, *Phys. Rev. Lett.* **49**, 841 (1982).
- [7] A. G. Zabrodskii, The Coulomb gap: The view of an experimenter, *Philos. Mag.* **B 81**, 1131 (2001); and references therein.
- [8] W. Mason, S. V. Kravchenko, G. E. Bowker, and J. E. Furneaux, Experimental evidence for a Coulomb gap in two dimensions, *Phys. Rev. B* **52**, 7857 (1995).
- [9] P. W. Anderson, Infrared Catastrophe in Fermi Gases with Local Scattering Potentials, *Phys. Rev. Lett.* **18**, 1049 (1967).
- [10] J. H. Davies, P. A. Lee, and T. M. Rice, Electron Glass, *Phys. Rev. Lett.* **49**, 758 (1982).
- [11] G. Vignale, Quantum electron glass, *Phys. Rev. B* **36**, 8192 (1987).
- [12] C. C. Yu, Time-Dependent Development of the Coulomb Gap, *Phys. Rev. Lett.* **82**, 4074 (1999).
- [13] M. Müller and L. B. Ioffe, Glass Transition and the Coulomb Gap in Electron Glasses, *Phys. Rev. Lett.* **93**, 256403 (2004).
- [14] E. Lebanon and M. Müller, Memory effect in electron glasses: Theoretical analysis via a percolation approach, *Phys. Rev. B* **72**, 174202 (2005); M. Müller and E. Lebanon, History depen-

- dence, memory and metastability in electron glasses, *J. Phys. IV France* **131**, 167 (2005).
- [15] V. Malik and D. Kumar, Formation of the Coulomb gap in a Coulomb glass, *Phys. Rev. B* **69**, 153103 (2004).
- [16] V. Malik and D. Kumar, Thermodynamics and excitations of Coulomb glass, *Phys. Rev. B* **76**, 125207 (2007).
- [17] A. Amir, Y. Oreg, and Y. Imry, Mean-field model for electron-glass dynamics, *Phys. Rev. B* **77**, 165207 (2008); Electron glass dynamics, *Annu. Rev. Condens. Matter Phys.* **2**, 235 (2011); Y. Meroz, Y. Oreg and Y. Imry, Memory effects in the electron glass, *Europhys. Lett.* **105**, 37010 (2014).
- [18] M. Pollak, M. Ortuño, and A. Frydman, *The Electron Glass* (Cambridge University Press, Cambridge, England, 2013).
- [19] Z. Ovadyahu, Slow dynamics of the electron-glasses: The role of disorder, *Phys. Rev. B* **95**, 134203 (2017).
- [20] G. Srinivasan, Statistical mechanics of charged traps in an amorphous semiconductor, *Phys. Rev. B* **4**, 2581 (1971).
- [21] A. Möbius, M. Richter, and B. Drittlar, Coulomb gap in two- and three-dimensional systems: Simulation results for large samples, *Phys. Rev. B* **45**, 11568 (1992).
- [22] M. Pollak, Effect of carrier-carrier interactions on some transport properties in disordered semiconductors, *Discuss. Faraday Soc.* **50**, 13 (1970).
- [23] A. Efros and B. Shklovskii, Coulomb gap and low temperature conductivity of disordered systems, *J. Phys. C: Solid State Phys.* **8**, L49 (1975).
- [24] E. Yamaguchi, H. Aoki, and H. Kamimura, Intra- and interstate interactions in Anderson localised states, *J. Phys. C: Solid State Phys.* **12**, 4801 (1979); H. Kamimura, Theoretical model on the interplay of disorder and electron correlations, *Prog. Theor. Phys. Suppl.* **72**, 206 (1982).
- [25] G. Massey and M. Lee, Direct Observation of the Coulomb Correlation Gap in a Nonmetallic Semiconductor, Si: B, *Phys. Rev. Lett.* **75**, 4266 (1995).
- [26] V. Yu. Butko, J. F. DiTusa, and P. W. Adams, Coulomb Gap: How a Metal Film Becomes an Insulator, *Phys. Rev. Lett.* **84**, 1543 (2000); V. Yu. Butko and P. W. Adams, Quantum metallicity in a two-dimensional insulator, *Nature (London)* **409**, 161 (2001).
- [27] A. Vaknin, Z. Ovadyahu, and M. Pollak, Non-equilibrium field effect and memory in the electron glass, *Phys. Rev. B* **65**, 134208 (2002).
- [28] U. Givan and Z. Ovadyahu, Compositional disorder and transport peculiarities in the amorphous indium-oxides, *Phys. Rev. B* **86**, 165101 (2012).
- [29] I. Zbeda, I. Bar, and Z. Ovadyahu, Microstructure and the boson peak in thermally treated InxO films, *Phys. Rev. Materials* **5**, 085602 (2021).
- [30] R. Wortis and W. A. Atkinson, Physical mechanism for a kinetic energy driven zero-bias anomaly in the Anderson-Hubbard model, *Phys. Rev. B* **82**, 073107 (2010).
- [31] R. Wortis and L. Mulindwa, Understanding disorder-induced zero-bias anomalies in systems with short-range interactions: An atomic-limit perspective, *Phys. Rev. B* **90**, 035101 (2014).
- [32] J. Mitchell, A. Gangopadhyay, V. Galitski, and M. Müller, Two-component Coulomb glass in insulators with a local attraction, *Phys. Rev. B* **85**, 195141 (2012).
- [33] F. Epperlein, M. Schreiber, and T. Vojta, Quantum Coulomb glass within a Hartree-Fock approximation, *Phys. Rev. B* **56**, 5890 (1997).
- [34] K. Driscoll, A. Ralko, and S. Fratini, Pseudogap metal induced by long-range Coulomb interactions, *Phys. Rev. B* **103**, L201106 (2021).
- [35] S. Levit and D. Orgad, Statistics of Hartree-Fock levels in small disordered systems, *Phys. Rev. B* **60**, 5549 (1999).
- [36] B. Surer, H. G. Katzgraber, G. T. Zimanyi, B. A. Allgood, and G. Blatter, Density of States and Critical Behavior of the Coulomb Glass, *Phys. Rev. Lett.* **102**, 067205 (2009).
- [37] A. Möbius and M. Richter, Comment on “Density of States and Critical Behavior of the Coulomb Glass,” *Phys. Rev. Lett.* **105**, 039701 (2010).
- [38] B. Surer, A. Glatz, H. G. Katzgraber, G. T. Zimanyi, B. A. Allgood, and G. Blatter, Surer *et al.* Reply:, *Phys. Rev. Lett.* **105**, 039702 (2010).
- [39] S. Akhanjee and J. Rudnick, Disorder Induced Transition into a One-Dimensional Wigner Glass, *Phys. Rev. Lett.* **99**, 236403 (2007).
- [40] S. Chakravarty, S. Kivelson, C. Nayak, and K. Voelker, Wigner glass, spin liquids and the metal-insulator transition, *Philos. Mag. B* **79**, 859 (1999).
- [41] R. Chitra, T. Giamarchi, and P. Le Doussal, Pinned Wigner crystals, *Phys. Rev. B* **65**, 035312 (2001).
- [42] L. F. Cugliandolo, T. Giamarchi, and P. Le Doussal, Dynamic Compressibility and Aging in Wigner Crystals and Quantum Glasses, *Phys. Rev. Lett.* **96**, 217203 (2006).
- [43] M. Amini, V. E. Kravtsov, and M. Müller, Multifractality and quantum-to-classical crossover in the Coulomb anomaly at the Mott-Anderson metal-insulator transition, *New J. Phys.* **16**, 015022 (2014).
- [44] D. C. Johnston, Stretched exponential relaxation arising from a continuous sum of exponential decays, *Phys. Rev. B* **74**, 184430 (2006).
- [45] Z. Ovadyahu, Slow conductance relaxations: Distinguishing the electron glass from extrinsic mechanisms, *Phys. Rev. B* **78**, 195120 (2008).
- [46] A. Vaknin, Z. Ovadyahu, and M. Pollak, Evidence for Interactions in Nonergodic Electronic Transport, *Phys. Rev. Lett.* **81**, 669 (1998).
- [47] The disorder that is required to localize the system is related to the competition with the system kinetic energy. It may therefore differ from that associated with the competition with the Coulomb interaction.
- [48] Z. Ovadyahu, Transition to exponential relaxation in weakly disordered electron glasses, *Phys. Rev. B* **97**, 214201 (2018).
- [49] A. Vaknin, Z. Ovadyahu, and M. Pollak, Temperature dependence of non-equilibrium effects in a Fermi-glass, *Europhys. Lett.* **42**, 307 (1998).
- [50] Z. Ovadyahu, Suppressing quantum effects by optically driven nonequilibrium phonons, *Phys. Rev. B* **103**, L100206 (2021).
- [51] I. M. Lifshitz and V. Y. Kirpichenkov, Tunnel transparency of disordered systems, *Zh. Eksp. Teor. Fiz.* **77**, 989 (1979) [*Sov. Phys. JETP* **50**, 499 (1979)].
- [52] M. Ya. Azbel, Eigenstates and properties of random systems in one dimension at zero temperature, *Phys. Rev. B* **28**, 4106 (1983).
- [53] J. B. Pendry, Quasi-extended electron states in strongly disordered systems, *J. Phys. C: Solid State Phys.* **20**, 733 (1987).
- [54] P. Charbonneau, A. Ikeda, G. Parisi, and F. Zamponi, Dimensional study of the caging order parameter at the glass transition, *Proc. Natl. Acad. Sci. USA* **109**, 13939 (2012); G. Biroli and

- J. P. Garrahan, Perspective: The glass transition, *J. Chem. Phys.* **138**, 12A301 (2013).
- [55] Z. Ovadyahu, Anisotropic magnetoresistance in a Fermi glass, *Phys. Rev. B* **33**, 6552 (1986); O. Faran and Z. Ovadyahu, Magneto-conductance in the variable range hopping regime due to a quantum interference mechanism, *ibid.* **38**, 5457 (1988); Z. Ovadyahu, Quantum coherent effects in Anderson insulators, *Waves in Random Media* **9**, 241 (1999).